ADVANCED ENERGY MATERIALS
www.advenergymat.de

Lithium Difluorophosphate-Based Dual-Salt Low Concentration Electrolytes for Lithium Metal Batteries

Hao Zheng, Hongfa Xiang, Fuyang Jiang, Yongchao Liu, Yi Sun, Xin Liang, Yuezhan Feng, and Yan Yu**

The safety hazards and low Coulombic efficiency originating from the growth of lithium dendrites and decomposition of the electrolyte restrict the practical application of Li metal batteries (LMBs). Inspired by the low cost of low concentration electrolytes (LCEs) in industrial applications, dual-salt LCEs employing 0.1 M Li difluorophosphate (LiDFP) and 0.4 M LiBOB/LiFSI/LiTFSI are proposed to construct a robust and conductive interphase on a Li metal anode. Compared with the conventional electrolyte using 1 M $LiPF_6$, the ionic conductivity of LCEs is reduced but the conductivity decrement of the separator immersed in LCEs is moderate, especially for the LiDFP–LiFSI and LiDFP–LiTFSI electrolytes. The accurate Coulombic efficiency (CE) of the Li‖Cu cells increases from 83.3% (electrolyte using 1 M $LiPF_6$) to 97.6%, 94.5%, and 93.6% for LiDFP–LiBOB, LiDFP–LiFSI, and LiDFP–LiTFSI electrolytes, respectively. The capacity retention of Li‖$LiFePO_4$ cells using the LiDFP–LiBOB electrolyte reaches 95.4% along with a CE over 99.8% after 300 cycles at a current density of 2.0 mA cm^{-2} and the capacity reaches 103.7 mAh g^{-1} at a current density of up to 16.0 mA cm^{-2}. This work provides a dual-salt LCE for practical LMBs and presents a new perspective for the design of electrolytes for LMBs.

H. Zheng, Prof. H. Xiang, F. Jiang, Y. Liu, Dr. Y. Sun, Dr. X. Liang
School of Materials Science and Engineering
Engineering Research Center of High Performance Copper Alloy Materials and Processing
Ministry of Education
Hefei University of Technology
Hefei, Anhui 230009, P. R. China
E-mail: hfxiang@hfut.edu.cn

Dr. Y. Feng
Key Laboratory of Materials Processing and Mold (Zhengzhou University)
Ministry of Education
Zhengzhou University
Zhengzhou 450002, P. R. China

Prof. Y. Yu
Hefei National Laboratory for Physical Sciences at the Microscale
Department of Materials Science and Engineering
CAS Key Laboratory of Materials for Energy Conversion
University of Science and Technology of China
Hefei, Anhui 230026, P. R. China
E-mail: yanyumse@ustc.edu.cn

Prof. Y. Yu
Dalian National Laboratory for Clean Energy (DNL)
Chinese Academy of Sciences (CAS)
Dalian 116023, P. R. China

The ORCID identification number(s) for the author(s) of this article can be found under https://doi.org/10.1002/aenm.202001440.

DOI: 10.1002/aenm.202001440

Lithium (Li) metal batteries (LMBs) are one of the most promising energy storage systems due to the extremely high theoretical specific capacity (3860 mAh g^{-1}) and the lowest standard redox potential (−3.040 V) of Li metal anode. Li metal was used early in Li secondary batteries by Professor Whittingham in the 1970s.[1] During the past four decades the rechargeable batteries with Li metal as anode have been studied extensively and especially the Li metal anode is indispensable in Li–sulfur (S) and Li–oxygen (O_2) batteries. The Li–S and Li–O_2 batteries deliver higher energy densities of 650 and 950 Wh kg^{-1}, respectively, than Li-ion batteries using graphite anode (about 250 Wh kg^{-1}).[2] Both are considered to be the most promising next generation energy storage systems. Nevertheless, the deployment of LMBs is hindered severely by the uncontrollable growth of Li dendrites and limited Coulombic efficiency (CE) during Li plating/stripping. During the plating step, Li is inclined to deposit in dendritic form owing to inhomogeneous current distribution, cation concentration gradient around the Li anode and the fracture of solid-electrolyte interphase (SEI).[3] Further plating and stripping progresses will result in the growth of dendritic Li. On one hand, the grown dendritic Li can penetrate the separator and bring about internal short circuits, which may cause thermal runaway and explosion hazards.[4] On the other hand, the exposure of fresh Li to electrolyte will lead to continuous formation of SEI on bulk Li anode, consumption of electrolyte and formation of isolated "dead" Li, which will render poor lifespan of the battery.[5]

Recently, the existing Li-ion batteries are gradually approaching the limits of their specific energy density, and increased efforts have been devoted to reviving the LMBs. Among diverse strategies the electrolyte engineering is one of the most practical and facile methods to stabilize the Li metal anode. Different additives have been developed to construct a stable SEI layer. Early researches demonstrated the successful applications of gaseous molecules (CO_2, SO_2) and liquid chemicals (2-methylfuran and its derivatives, vinylene carbonate and fluoroethylene carbonate) in protection of Li anode.[6] Many new additives have been developed recently, such as $CsPF_6$, trimethylsilyl azide, RbF, hexafluoroacetylacetone, and Li trifluoro(perfluoro-*tert*-butyloxyl) borate, and even increased the CE of Li‖Cu cells up to 99%.[7] High concentration

electrolytes (HCEs) also received much attention as a very promising strategy in recent years. Increasing the molar ratio of Li salt to solvent not only enhances the solvent coordination, but also regulates the interfacial chemistry on the anode surface, which may suppress the degradation of Li metal and electrolyte during extended cycling.[8] Furthermore, HCEs also exhibit improved oxidative stability and nonflammability.[9] The electrolyte composed 4 M Li bis(fluorosulfonyl)imide (LiFSI) in 1,2-dimethoxyethane (DME) demonstrates a high CE of 99.8% up to 4.5 V for the Li‖$Ni_{1/3}Co_{1/3}Mn_{1/3}O_2$ cells.[10] However, several critical defects hinder the practical applications of HCEs, including high viscosity, poor wettability to separator and cathode, and poor performance at low temperature.[11] Especially, the cost of Li salt accounts for more than 50% of the electrolyte cost in practical production, so increasing the salt concentration greatly increases the cost of the electrolyte. Localized high concentration electrolytes (LHCEs) have been proposed to conquer these issues. In the LHCE, a cosolvent which is hardly involved in the solvation structures is introduced into the HCE to reduce the content of Li salt but maintain anodic stability.[12] For other studies on electrolytes, it was reported that in an electrolyte with a Li salt concentration of 1 M, appropriately increasing the discharge current to 2–4 mA cm^{-2} could form a transient high-concentration electrolyte layer on the surface of Li anode, which reduced the side reactions between the free organic solvents and Li metal anode and improved the lifespan of the battery.[13] Further reducing the salt concentration has been proven to be feasible in sodium-ion batteries. The electrolyte with 0.3 M $NaPF_6$ improved the stability of sodium-ion batteries over a wide temperature range because of the low viscosity and less HF corrosion at low and high temperatures, respectively.[14] While reducing the content of Li salt was rarely reported but worth considering from the perspective of application, especially for the Li or Na metal batteries with high energy densities.[15]

Similar to the reduced conductivity of the electrolyte with increasing the salt concentration over 1.5 M, reducing the salt concentration below 1 M will also lead to the decrease of ionic conductivity, whereas the diffusion coefficient of Li^+ ion in low concentration electrolyte (LCE) is much higher than that in HCE (Figure S1, Supporting Information).[16] The low interface resistance and the high transference number enable a concentrated electrolyte to be used in LMBs successfully, despite its low conductivity.[10] Therefore, the conductivity does not completely determine the application of the electrolyte, and the ability to form a stable SEI layer is decisive. Based on this principle, designing an LCE that can form a robust SEI layer could also improve the compatibility of the electrolyte with the Li anode. Moreover, the superiorities of high diffusion coefficient and low cost endow the LCE with practical application perspective. However, the SEI layer formed in the carbonate electrolytes with $LiPF_6$ concentration less than 3 M is usually dominated by the species derived from the decomposition of electrolyte. This organic SEI layer is porous and soluble and could not prevent the bulk Li from further corrosion.

In this paper, we do not simply reduce the concentration of Li salts, but apply dual-salt for modifying the SEI chemistry on Li anode. Dual-salt electrolytes adopting at least one salt capable of passivating Li metal anode have been extensively investigated. Jiao et al. reported that the Li‖$Ni_{1/3}Co_{1/3}Mn_{1/3}O_2$ cells delivered a high capacity retention of 90.5% after 300 cycles in the dual-salt electrolyte composed of 2 M Li bis(trifuoromethanesulfonyl) imide (LiTFSI) and 2 M Li difluoro(oxalato)borate (LiDFOB).[17] Our previous work also explored the effect of dual-salt electrolyte of LiTFSI and Li bis(oxalato)borate (LiBOB) in esters on improving the stability of SEI on Li anode.[18] LiBOB and LiTFSI improved the stability and ionic conductivity of SEI, respectively. The synergistic effect of both salts contributed to a robust and conductivity SEI rich in Li oxalate, boron semicarbonate-like species and sulfonate species. Furthermore, LiBOB also inhibited the corrosion of Al foil by LiTFSI. Consequently, the Li‖Li $Ni_{0.8}Co_{0.15}Al_{0.05}O_2$ cell in the dual-salt electrolyte demonstrated an improved capacity retention up to 80% compared with that of the cell in the conventional $LiPF_6$ electrolyte (15%) and the surface film impedance and voltage difference decreased a lot for the dual-salt electrolyte. Further adding 0.05 M $LiPF_6$ into this LiTFSI–LiBOB dual-salt electrolyte promoted the formation of polycarbonates, which bind other SEI compounds and isolated Li together and stick them to the Li metal anode.[19] Under the protection of the reinforced SEI, the Li‖$LiNi_{0.4}Co_{0.2}Mn_{0.4}O_2$ cells could survive up to 450 cycles at 1.75 mA cm^{-2} in the electrolyte using 0.6 M LiTFSI and 0.4 M LiBOB. Successful application of dual-salt electrolytes has been verified under high and conventional concentrations but the feasibility of dual-salt electrolytes under low concentrations is still rarely discussed. Li difluorophosphate (LiDFP) as an emerging salt can passivate the interphase of the high-voltage cathode and graphite.[20] Moreover, our team also explored the potential benefit of LiDFP on Li metal anode.[21] The decomposition of LiDFP helped generate an SEI rich in LiF and P–O species. The LiF improved the rigidity of SEI and promoted the kinetics of Li^+ ion diffusion and the P-O species was also beneficial for the Li^+ ion transfer. The resultant SEI layer was compact and conductive, thus low polarization was observed in Li‖Li symmetric cells and high accurate CE approaching 95.2% was reached in Li‖Cu cells using carbonate solvents containing 0.15 M LiDFP. Herein, we design several low concentration dual-salt electrolytes consisting of 0.1 M LiDFP and 0.4 M LiBOB, LiFSI, or LiTFSI in ethylene carbonate (EC) and dimethyl carbonate (DMC) (3:7 by weight ratio) (abbreviated as D4B, D4F, and D4T). The electrolyte using 1 M $LiPF_6$ is used as standard electrolyte (abbreviated as STD). The ionic conductivity, separator wettability, CE of Li plating/stripping, components of SEI, and cycling performance of LMBs have been systematically investigated for the LCEs. This work reports the application of low-cost dual-salt LCEs in LMBs for the first time, deepening the understanding of salt concentration and providing more experience to promote the practical application of LMBs.

Although the weight ratio of Li salt is only around 10% in the electrolyte, the cost of Li salt usually accounts for more than 50% of the total electrolyte cost due to the high unit-price of Li salt (Figure S2 and Table S1, Supporting Information). Considering the similar unit-price of different salts, using LCEs could reduce the cost of Li salt to 60% (Table S2, Supporting Information). First, the effect of reducing the concentration of Li salt on the physical properties of electrolyte is investigated. Ionic conductivity is one of the most important physical properties of an electrolyte. Reducing the concentration of Li salt to half of

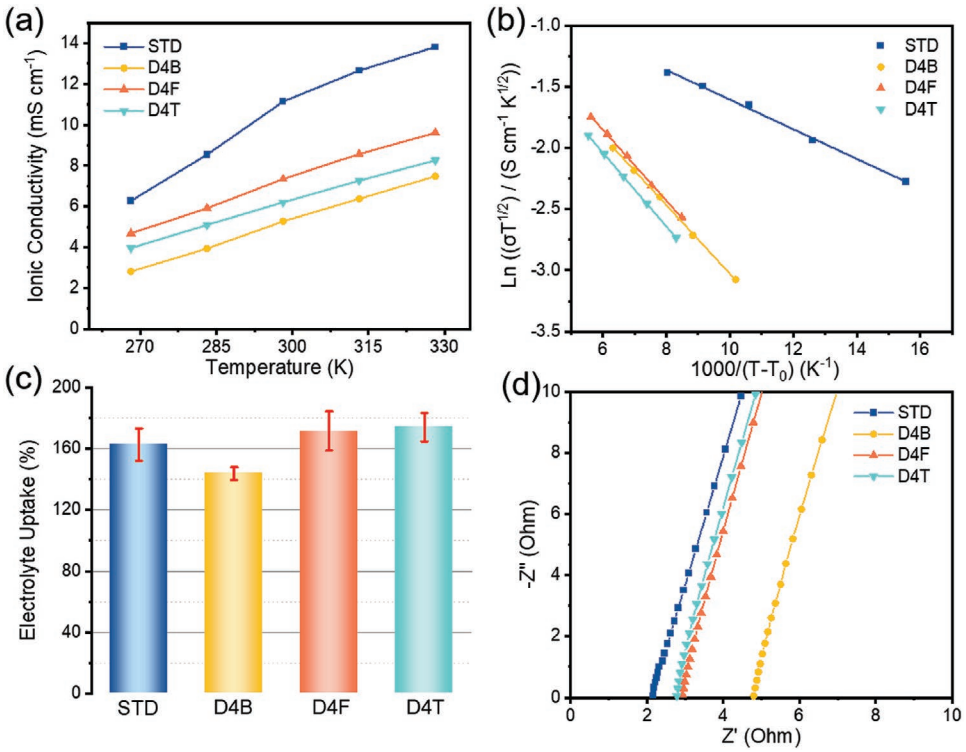

Figure 1. a) Ionic conductivity of electrolytes in the temperature range of 268.15 to 328.15 K and b) presented with VTF plots. c) Electrolyte uptake of the electrolytes toward PE separator and electrochemical impedance spectra of the SS|wet separator|SS symmetric cells.

the conventional electrolyte will definitely lead to conductivity decrement, as shown in **Figure 1**a. Different salts have a great impact on the electrolyte conductivity and its sensitivity to temperature. At room temperature (298.15 K), the STD electrolyte demonstrates the highest ionic conductivity of 11.14 mS cm^{-1}. Among the LCEs, D4B electrolyte shows the lowest conductivity of 5.27 mS cm^{-1}, which was only 48% of the conductivity of the STD electrolyte. Meanwhile D4F and D4T electrolytes show slightly higher conductivity of 7.35 and 6.21 mS cm^{-1}, respectively, which are 67% and 57% of the conductivity of the STD electrolyte. The sensitivity of conductivity to temperature is different in these electrolytes, as shown in Figure 1b. Vogel–Tamann–Fulcher (VTF) equation can be used to describe the temperature dependence of the conductivity of the complex system. According to the VTF equation, $\ln(\sigma T^{1/2})$ has a linear relationship versus $(T–T_0)^{-1}$. The values of T_0 and E_a fitted according to the VTF equation are shown in **Table 1**. The figure of $\ln(\sigma T^{1/2})$ versus $(T–T_0)^{-1}$ is fitted well linearly using the T_0 values shown in the table. The STD electrolyte has the lowest E_a, indicating that its conductivity is relatively less sensitive to temperature, which is consistent with the low slope of the STD in VTF plots.

In the battery, the medium for Li ion transport is not merely the electrolyte, but also the separator wetted by the electrolyte. Therefore, the wettability of the electrolyte toward the separator and the conductivity of the wet separator have important effects on the actual transfer process of Li^+ ion.[22] The separator wettability as well as the conductivity of the wet separator shows the superiority of the LCEs compared with HCEs. The electrolyte uptake is one of the most important indexes to characterize the wettability of the electrolyte toward the separator. The electrolyte uptake of polyethylene (PE) separator used in this paper is shown in Figure 1c. All electrolytes demonstrate a moderate electrolyte uptake over 130%, indicating good wettability toward the nonpolar PE separator, because the solvents blended of linear and cyclic carbonates possess low viscosity and polarity.[23] The electrolyte uptake of the B4B electrolyte is 143.7%, lower than that (162.2%) of the STD electrolyte. Whereas the electrolyte uptakes of D4F and D4T electrolytes are much higher and reach 171.5% and 174.1%, respectively.

Table 1. Ionic conductivities of electrolytes and wet separators at room temperature (298.15 K) and the fitting results of VTF equation.

Electrolyte	R_b [Ω]	σ_s [mS cm^{-1}]	σ_e [mS cm^{-1}]	MacMullin number	T_0 [K]	E_a [kJ mol^{-1}]
STD	2.15	0.348	11.14	31.96	203.8	1.01
D4B	4.79	0.156	5.27	33.67	170.0	2.33
D4F	2.93	0.256	7.35	28.73	150.4	2.41
D4T	2.78	0.270	6.21	23.03	147.8	2.51

The impedance of the wet separator is shown in Figure 1d and Table 1. Basically, the oblique line reflects the electric double layer behavior at the electrode/electrolyte interphase, and the ohmic impedance of the wet separator can be obtained from the intercept of the X axis. The conductivity of the wet separator is governed by the bulk conductivity of the electrolyte and the separator wettability, which are both dominated by the Li salt used. The separator absorbing the STD electrolyte shows the highest ionic conductivity of 0.35 mS cm^{-1}. The conductivity of the separator in D4B, D4F and D4T electrolyte is 0.16, 0.26, and 0.27 mS cm^{-1}, respectively, which is correspondingly 44.8%, 73.6% and 77.6% of that in STD electrolyte. In terms of the ratio of electrolyte conductivity (σ_e) and separator conductivity (σ_s) between LCEs and STD electrolyte, the ratio of σ_s is lower than σ_e between D4B and STD electrolyte, while that of D4F and D4T is in the opposite. This proves that D4B electrolyte has poor wettability and D4F and D4T have better wettability compared with the STD electrolyte. MacMullin number as a parameter reflecting the separator wettability is calculated to exclude the effect of conductivity difference. Basically, a smaller MacMullin number indicates better wettability.[24] The MacMullin number of D4B (33.67) is higher than that of STD electrolyte (31.96). While MacMullin number of D4F (28.73) and D4T (23.03) is much lower. This further confirms the difference in wettability of different electrolytes toward PE separators. The better wettability of D4T electrolyte is mainly due to the higher affinity between the nonpolar $-CF_3$ groups in LiTFSI and nonpolar PE separators.[25] Transference number of Li^+ ions (t_+) in STD, D4B, D4F, and D4T electrolyte is 0.37, 0.49, 0.58, and 0.50, respectively (Figure S3, Supporting Information). The higher t_+ of the LCEs indicates that the LCEs is favorable for Li^+ ions transfer, which will reduce the concentration polarization and even parasitic reactions with active electrodes.[26]

The frontier molecular orbital energies were calculated to predict the reductive stability of various salts and the role of salt on building the SEI layer. For the molecule with a higher highest occupied molecular orbital (HOMO) energy, the electron in the outermost layer has higher energy and tends to be lost more easily under high voltage, resulting in the oxidization of the molecule at a lower voltage. For the molecule with a lower lowest unoccupied molecular orbital (LUMO) energy, the innermost unoccupied electron orbital is lower, and foreign electrons are more likely to occupy this orbital, resulting in the reduction of the molecule at a higher voltage. Chemical hardness (η) related to the relative reactivity of the molecule is calculated as the mean of HOMO and LUMO energy.[27] Low η indicates that the molecule is more likely to decompose, which is a favorable feature for film-forming additives.[28] The frontier molecular orbital energies of the anions and LiDFP molecule are shown in **Figure 2**a. Obviously, PF_6^- has the highest LUMO energy (0.42 eV) and η (5.25 eV), which means that PF_6^- is the most difficult to be reduced compared with other molecules. It should be noted that even if PF_6^- has a relatively high reductive stability, it is still thermodynamically unstable on the Li metal anode. Although all the salts here are thermodynamically unstable on Li anode, a stable SEI layer formed by the pre-reduced salts can effectively inhibit the kinetic process of salt decomposition. BOB^- has the lowest LUMO energy (–2.14 eV) and η (2.87 eV), which is consistent with the well-known situation that LiBOB can be used as a film-forming additive. FSI^- and $TFSI^-$ have similar η (3.96 and 3.97 eV). However, the LUMO energy of $TFSI^-$ (0.10 eV) is much higher than that of FSI^- (–0.28 eV), which means that FSI^- is more prone to be reduced and participates in the formation of SEI layer. Compared with FSI^- ion, DFP^- has similar η (3.94 eV), but a higher LUMO energy (0.22 eV). In contrast, LiDFP has a similar η (3.99 eV), while its LUMO can be reduced to –0.23 eV, showing a more reducible property. Considering the low solubility of LiDFP (about 0.17 M in EC/DMC solvents), we speculate that some DFP^- will associate with Li^+ ion to form LiDFP after adding another salt. Then LiDFP undergoes a reductive decomposition on the surface of Li metal surface. BOB^- and FSI^- may also participate in the formation of SEI layer for their lower η and LUMO energy.

The accurate CE of the Li||Cu cells was measured to determine the compatibility of the electrolyte with the Li metal anode, and the results are shown in Figure 2b and Figure S4 (Supporting Information). The CE of STD electrolyte is only 83.3% due to the continuous side reactions resulted from the insufficient protection of SEI layer for Li metal. D4B electrolyte shows a relatively higher CE of 97.6%, because LiDFP and BOB^- may synergistically form a robust SEI layer. The CE of D4F electrolyte (94.5%) is slightly higher than that of D4T electrolyte (93.6%), which may attribute to the enhanced SEI layer modified by FSI^-. Figure 2c shows the cycling stability of Li||Li symmetric cells with various electrolytes at 0.5 mA cm^{-2}. In the initial stage, the plateau voltage in D4B corresponding to Li deposition is actually higher than that in STD due to the low conductivity of D4B, but the voltage fluctuation for STD is higher. Hence the overpotential of STD looks higher in the overview. In the later cycles, due to the instability of the SEI formed in STD, the electrolyte undergoes continuous decomposition, and the decomposition products adhere to the surface of Li metal. As a result, the transmission of Li^+ ions is hindered and the overpotential increases rapidly. The cells with all LCEs exhibit stable cycling profiles over 280 h. The D4B electrolyte shows a higher overpotential in the initial stage due to the low bulk conductivity of the D4B electrolyte and the overpotential gradually decreases as the cycling proceeds resulted from the rearrangement of the components and structure of the SEI layer, but it is still higher than the overpotential of the D4F and D4T electrolytes.

To disclose the morphologies and the components of SEI on Li anode, Li metal retrieved from Li||Cu and Li||Li cells were investigated by scanning electron microscope (SEM) and X-ray photoelectron spectrometer (XPS). Figure S5 (Supporting Information) shows the morphologies of Li deposited on Cu foil with an areal capacity of 1.5 mAh cm^{-2}. In the STD electrolyte, large amount of Li dendrites with a loose structure are observed. On one hand, dendritic Li increases the specific surface area of the Li metal anode, intensifies the side reactions between the electrolyte and the Li metal, and leads to low CE. On the other hand, Li dendrites may penetrate the separator and cause safety hazards. In contrast, the Li metal deposited in the LCEs demonstrates a dense and nodule-like morphology without any dendrites. This proves that the LCEs designed possess higher compatibility to the Li anode with fewer side reactions. The deposited Li in D4B electrolyte is compactly integrated with the

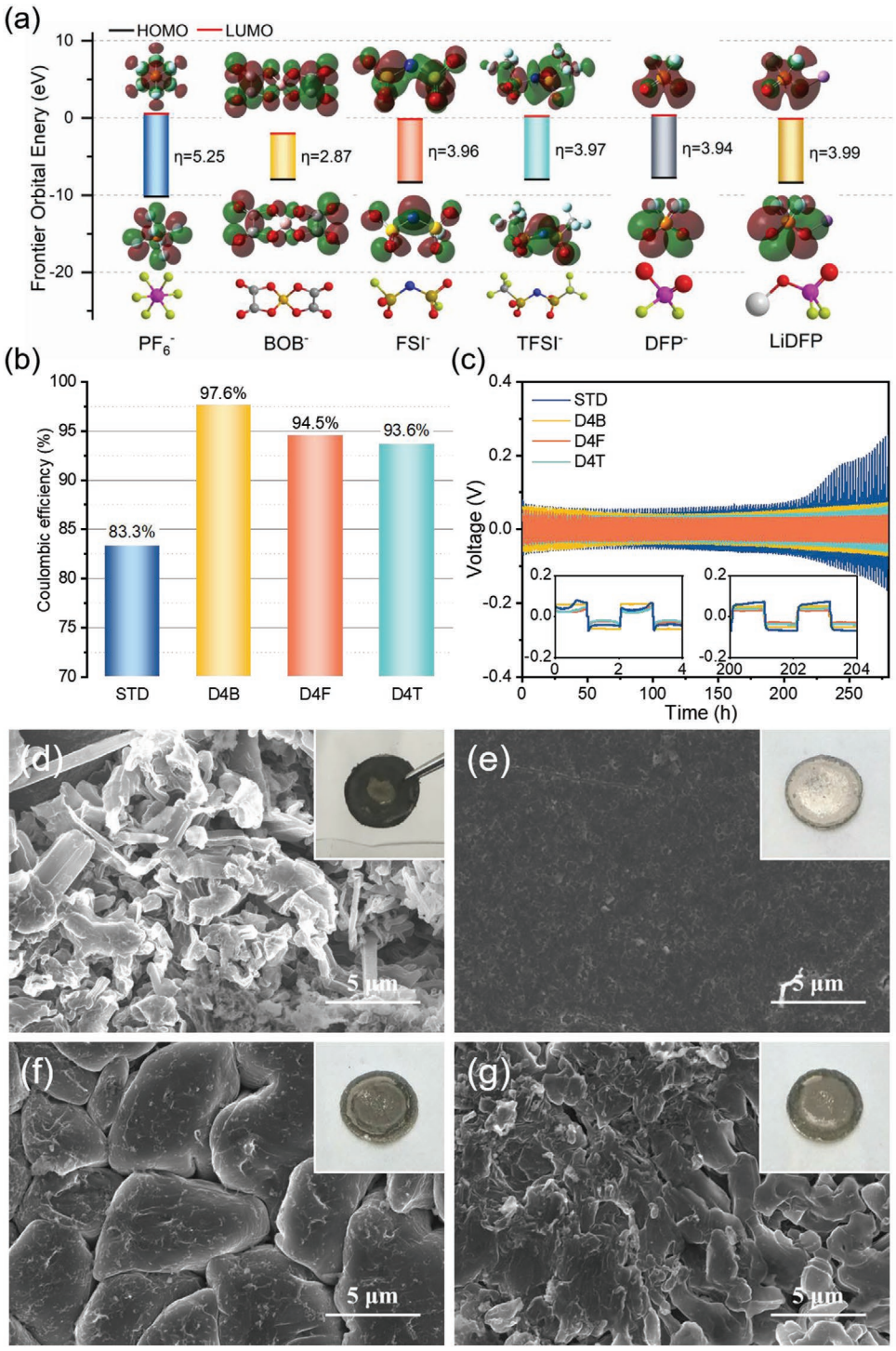

Figure 2. a) Frontier molecular orbital energies of the anions used and the LiDFP molecule. b) Average CE of Li||Cu cells and c) the cycling performance of Li||Li symmetric cells at the current density of 0.5 mA cm^{-2} with a capacity of 0.5 mAh cm^{-2}. Morphologies of the Li metal harvested from the Li||Li symmetric cells after cycling in d) STD, e) D4B, f) D4F, and g) D4T electrolytes. The insets are the optical images of Li metal retrieved from Li||Li cells.

best uniformity. In D4F and D4T electrolytes, Li anode morphologies are slightly porous but large piece of nodule-like Li is also observed, which is apparently different from the needle-like Li deposited in the STD electrolyte. The pristine Li demonstrates a compact morphology with some wrinkles (Figure S6, Supporting Information). Figure 2d–f shows the optical images (the image inset) and surface morphology of Li metal after cycling in Li||Li symmetric cells. There are a large number of black deposits on the surface of the Li metal after cycling in STD electrolyte, which are the decomposition products of the

electrolyte and dead Li. The SEM image shows that the anode is pulverized and porous, and the surface of Li is needle-like, which demonstrates that the protection of fresh bulk Li is insufficient. As a sharp contrast, Li metal anode with similar silvery luster to the pristine Li is observed in the D4B electrolyte. The deposits are rarely observed and the Li anode exhibits a very smooth and uniform surface morphology. The uniform morphology is attributed to the conductive and structural uniform SEI film formed by LiDFP and BOB^- synergistically. The structural uniformity is critical to the durability of the SEI and uniform deposition of Li^+ ion, which eventually leads to the best cycling stability among all electrolytes.[29] There is a small amount of decomposition products of the electrolyte depositing on the surface of Li metal cycling in D4F and D4T electrolytes and both demonstrate uniform and compact morphology. Nevertheless, the specific shape of the Li deposited is different. The morphology of Li metal in D4F electrolyte is nodule-like with a larger size and the Li metal in D4T electrolyte is granular-like and smaller. Different deposition morphologies are caused by the different characteristics of the SEI films formed, whereas the stability of SEI film formed in D4F and D4T is not as compact and stable as that formed in D4B electrolyte.

Furthermore, the components of the SEI film formed on Li anode after cycling in Li‖Li symmetric cells was investigated by XPS, as shown in **Figure 3**. In the C 1s spectra, four peaks derived from electrolyte decomposition, $ROCO_2Li$ (289.9 eV), C=O (288.4 eV), C—O (286.4 eV), and C—C/C—H (284.8 eV) are observed in STD electrolyte. In the D4B electrolyte, the C=O and C—O peaks are significantly enhanced, which is due to the decomposition of BOB^-. In D4T and D4F electrolytes, the intensity of the C 1s spectra is significantly reduced, indicating the suppression of electrolyte decomposition to some extent. The two peaks of $Li_xPO_yF_z$ (686.8 eV) and LiF (684.7 eV) dominate the F 1s spectrum, which are both originated from the decomposition of $LiPF_6$ or LiDFP. Generally, the diffusion of Li^+ ions in the inorganic grain boundary (e.g., LiF, $LiNO_3$) is fast and LiF has high shear modulus (55.1 GPa).[5b,30] Therefore, the higher LiF content is beneficial to the rapid transfer of Li^+ ions, improving the hardness of the SEI film and suppressing the formation of Li dendrites. The content of $Li_xPO_yF_z$ in the SEI film decreases significantly while the content of LiF increases significantly after the introduction of LiDFP. The relatively high LiF content is beneficial to the kinetics of Li^+ ions transfer, improves the uniformity of Li deposition, and results in dendrite-free morphology. The increased intensity of LiF is the direct evidence of the reduction of LiDFP on Li anode, and it is further verified by the contrast of P 2p spectra. The P 2p spectra of the LCEs quite differ from the STD electrolyte. The peak located at 686.8 eV is for $Li_xPO_yF_z$ and a new peak located at 684.7 eV for P–O is observed on the surface of the Li metal after cycling in LCEs, both of which are derived from the decomposition of LiDFP. The increasing content of P–O compounds also benefits the kinetics of Li^+ ions transfer in the SEI film, improves the toughness of the SEI film, and suppresses the growth of dendrites and their reactions with electrolytes.[20b]

In addition, B 1s and N 1s spectra were analyzed to determine whether BOB^-, FSI^-, and $TFSI^-$ contributed to the formation of the SEI film (Figure S7, Supporting Information). In the B 1S spectrum of the D4B electrolyte, the Li–B–O peak located at 193.4 eV and the B–O peak located at 192.2 eV are observed, which confirm that some BOB^- decomposed to produce the SEI film. The B–O bond is broken via a ring-opening reaction in the electrochemical decomposition.[31] The decomposition products composed of carbonyl moieties and Li_2BO_x contribute to the formation of the SEI film. Li_2BO_x is less soluble and exhibits stronger coordination to semicarbonates compared with other inorganic ions in the SEI film (LiF, $LiCO_2$, and Li_2O), which suppressed the dissolution of the organic species located on the outer layer of the SEI film.[32] The suppressed dissolution of organic compounds endows the SEI film with better flexibility and structural uniformity to accommodate the deformation of Li anode surface. The resultant stable and flexible SEI layer ensures the uniform and dendrite-free morphology of deposited Li, as shown in Figure 2e. The stable SEI layer even enables the Li‖Li cells to cycle more than 400 h at 1 mA cm^{-2} and 1 mAh cm^{-2}, whereas the cell in STD electrolyte becomes short circuit only after 90 h (Figure S8, Supporting Information). In the N 1s spectrum of the D4F electrolyte, a weak Li–N peak related to Li_3N and $Li_2N–SO_2^-$ species is observed at 398.8 eV, which is not detected in the D4T electrolyte.[33] This indicates that a small amount of FSI^- decomposes to form the SEI film, but $TFSI^-$ dose not. The content of LiF is slightly higher due to the decomposition of FSI^-. The LiF and nitrogen compounds stabilize the SEI layer hence the D4F electrolyte demonstrates better compatibility with Li metal than D4T electrolyte.

In order to further probe the practicality of LCEs, the cycling and rate performances of Li‖$LiFePO_4$ (LFP) cells with moderate high cathode capacity (2.0 mAh cm^{-2}) were investigated. **Figure 4**a shows the cycling stability of the LMBs at 1C after two formation cycles at 0.1C. The LMB using STD electrolyte experiences a rapid capacity degradation after 70 cycles accompanied by a low CE. The capacity retention was only 11.6% with an average CE of 97.8% after 300 cycles. This poor cycling stability is ascribed to the poor compatibility between the electrolyte and Li metal. Due to the relatively high capacity utilization of the cathode, the large volume change and the formation of Li dendrites cause the break of SEI film continuously. Fresh Li directly contacts the electrolyte and the electrolyte is quickly consumed owing to the intensified parasitic reaction. As a result, the battery fails quickly with low CE. In the case of LCE, only slightly capacity loss is observed. The capacity retention of cells using D4B, D4F and D4T electrolytes is increased to 95.4%, 94.9%, and 90.7%, respectively, with an average CE exceeding 99.8%. Note that the capacity of the cells in D4T electrolyte begins to decline significantly after 270 cycles, indicating the degradation of SEI layer. The representative voltage profiles of Li‖LFP cells are demonstrated in Figure 4c-f. The first circle of the cell using STD electrolyte shows the highest specific discharge capacity (161.6 mAh g^{-1}), but the lowest CE (98.7%). This originates from the inherently higher conductivity but more side reactions of the electrolyte. As the cycle progresses, a rapid decay in capacity and a rapid increase in overpotential are observed owing to the continuously increased internal resistance. The CE of the cells in D4B, D4F and D4T electrolytes is improved to 101.1%, 100.4%, and 100.8%, respectively. The CE above 100% is attributed to the slightly Li deficiency in the cathode formed due to the Li volatilization during sintering process. From the 50th to the 300th cycle, the cells in the D4B

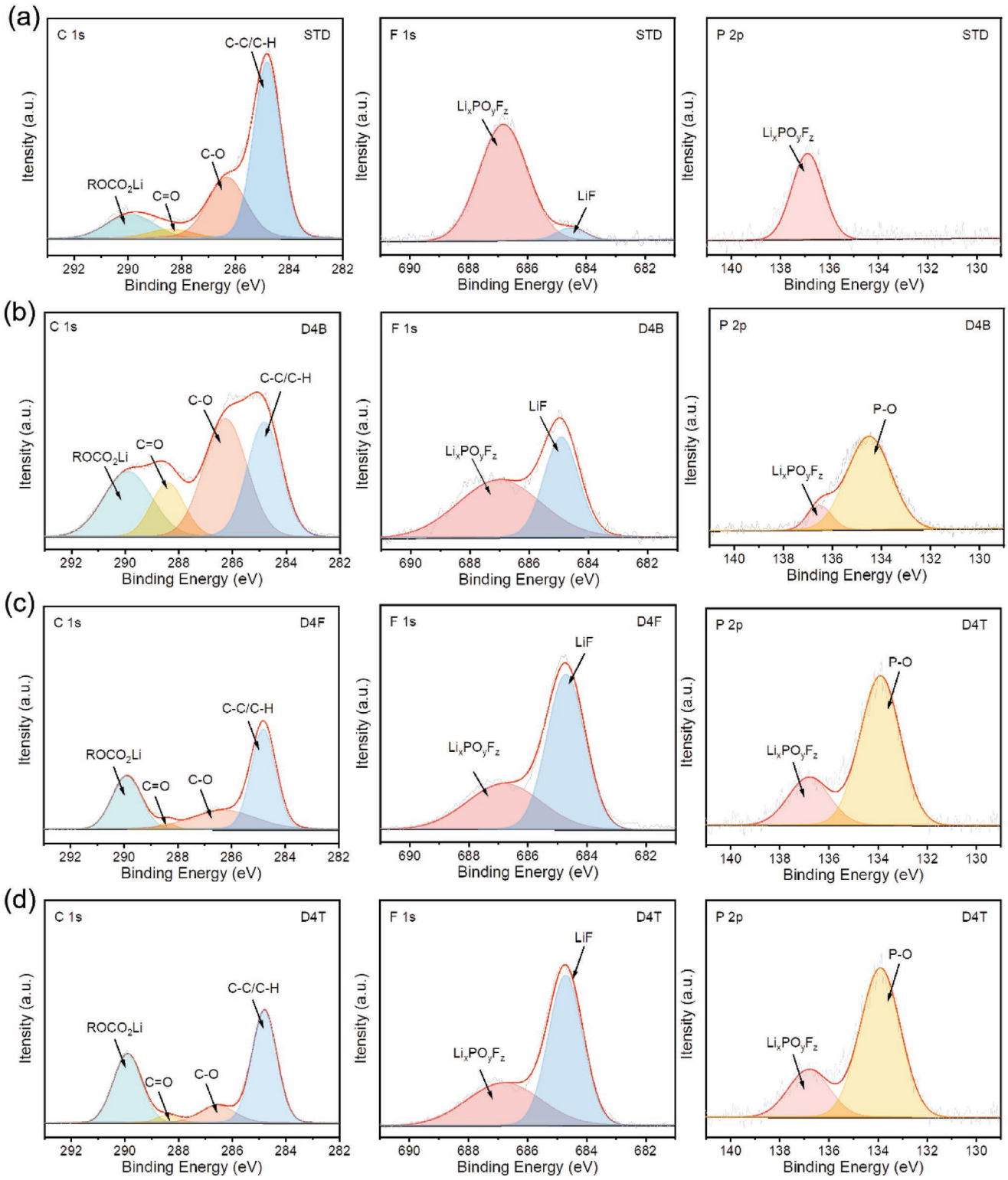

Figure 3. The C 1s, F 1s, and P 2p XPS spectra of the Li metal electrolyte retrieved from the Li||Li symmetric cells after cycling in a) STD, b) D4B, c) D4F, and d) D4T electrolytes.

and D4F electrolytes show lower capacity attenuation and overpotential, while the capacity attenuation and overpotential of the cell using D4T electrolyte are slightly higher. This may be due to slightly weakened interfacial compatibility between the anode and D4T electrolyte. Figure 4b shows the rate performance of the LMBs. All cells exhibit similar capacities

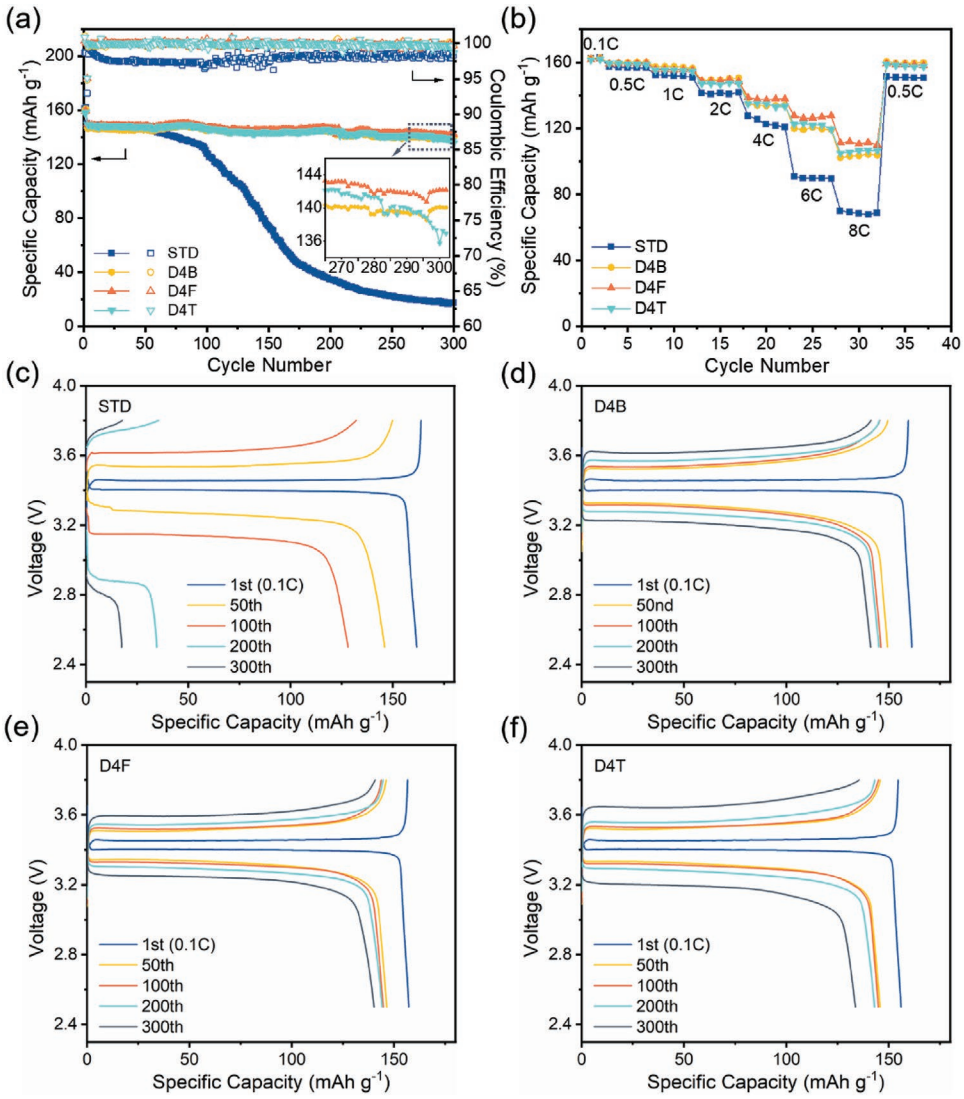

Figure 4. a) Cycling and b) rate performance of the Li||LFP cells. The representative voltage profiles of Li||LFP cells using c) STD, d) D4B, e) D4F, and f) D4T electrolytes.

when the current density is lower than 1C. As the current increases, the specific capacity of the cell using STD electrolyte decays rapidly. The capacity of the cell using STD electrolyte also decreases at a constant current density. This is due to the large amount of electrolyte decomposition on the Li metal anode, which increases the internal resistance of the cell. Furthermore, after the current density is reset to 0.5C after 8C tests (16 mA cm^{-2}), the specific capacity of Li||LFP cell in STD electrolyte cannot be totally recovered. Under the rate of 8C, D4B, D4F, and D4T electrolytes can maintain specific capacity of 103.7, 109.9, and 106.5 mAh g^{-1}. Low capacity of the cell in D4B is attribute to the low ionic conductivity of D4B electrolyte. The full recovery of the specific capacity of the cells in LCEs at 0.5C demonstrates the enhanced reversibility. Comparison of the performance of 0.5 and 1 M $LiPF_6$ electrolytes confirms that it is the SEI layer rather than ionic conductivity that governs the cell performance (Figure S9, Supporting Information). The stable cycling performance of D4B electrolyte with a Li foil of 100 µm further validate the practicality of LCE (Figure S10, Supporting Information).

The AC and DC impedances were tested to characterize the internal resistance of Li||LFP cells (Figures S11 and S12, Supporting Information). AC impedance spectra demonstrate that after 2 formation cycles all cells exhibit similar ohmic impedance. The cell in D4B electrolyte exhibits the highest total impedance, while the cell in STD electrolyte exhibits the lowest total impedance. After 100 cycles, the impedance of the cells in LCEs gradually decreases to a similar value, while the impedance of the STD electrolyte increases continuously, implying that the SEI film formed in LCEs is more stable and protects the Li metal from the corrosion of the electrolyte. The DC impedance spectra during the charging progress are shown in Figure S12c,d (Supporting Information). After 2 formation cycles, there is sufficient electrolyte in all batteries. Therefore, the content of Li^+ ions in the solution is enough to supplement the consumption of Li^+ ions on the electrode surface

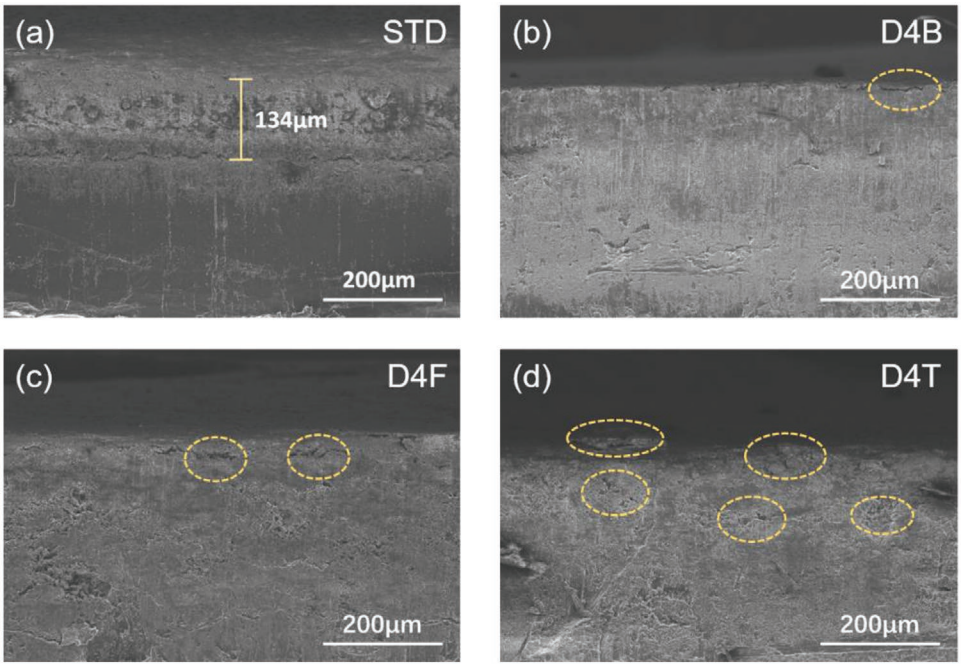

Figure 5. Cross-section views of cycled Li recovered from Li‖ LFP cells after 300 cycles in a) STD, b) D4B, c) D4F, and d) D4T electrolytes.

and maintain a low concentration polarization. As a result, all electrolytes exhibit low DC impedances. After 100 cycles, due to the large consumption of STD electrolyte in the cell, there are fewer Li^+ ions left in the electrolyte. A large concentration polarization is established during charging progress, exhibiting a significantly increased DC impedance. Conversely, the Li loss in the LCEs is small, and the low concentration polarization maintained results in low DC impedance. The Li vacancies in the cathode become fewer with the increase of the capacity, which makes the insertion of new Li more difficult, and makes the DC impedance increase with the capacity.

The cross-section images of the Li metal harvested from the Li‖LFP cells after 300 cycles were characterized by scanning electron microscopy (SEM) to obtain a better understanding of the cycling stability of the cells using LCEs, as shown in **Figure 5**. The cross-section views of the cycled Li anode in the STD electrolyte shows a very significant cracks at the depth of 133.9 μm in the bulk Li. The Li above this crack shows a loose corrosion layer, which mainly contains the decomposition products of the electrolyte and dead Li. Such a thick corrosion layer undoubtedly consumes a large amount of electrolyte and fresh Li, causing a dramatic increase in internal resistance and ultimate failure. On the contrary, the Li anode recovered from D4B electrolyte exhibits smooth surface along with dense and uniform bulk with no significant corrosion and cracks. The D4B electrolyte derived SEI suppresses the growth of Li dendrites and parasitic reactions, demonstrating the efficacy of this electrolytes. As for the Li metal cycled in D4F and D4T electrolytes, there are some porous blocks near the surface, especially in the D4T electrolyte, indicating the insufficient protection of SEI film. The stable performance of Li‖LFP cells and dense morphology of Li metal verify the compatibility of LCEs toward Li anode, but the oxidative stability of D4B is unsatisfactory and D4F and D4T electrolytes could corrode Al foil extensively, which restrict the application of LCEs for high voltage cathode (Figures S13 and S14, Supporting Information).

The positive effect of low concentration D4B electrolyte on the interphase of Li metal anode is summarized in **Figure 6** based on the results and discussions mentioned above. When the cycling is performed in the $LiPF_6$ electrolyte, the SEI layer derived from the decomposition of $LiPF_6$ and solvents is loose and less conductive. As the volume of the anode changes during cycling, the SEI film undergoes repeated cracking-reparation processes continuously. Li dendrites are constantly formed and the direct contact between fresh Li and the electrolyte leads to a large number of side reactions and rapid consumption of electrolyte, which ultimately lead to safety hazards and short lifespan of the battery. As for the D4B electrolyte, LiDFP contributes to the formation of an SEI film rich in LiF and phosphate compounds, improving the conductivity of the SEI film. Additionally, BOB^- also decomposed to produce carbonyl moieties and Li_2BO_x. The Li_2BO_x demonstrates better coordination with semicarbonates compared with other inorganic species in SEI. Thus, dissolution of organic species in the outer layer of the SEI film is suppressed. The resultant SEI exhibits improved structural uniformity and flexibility, and can accommodate the volume changes of Li metal. Under the protection of a conductive and flexible SEI film, uniform Li platting and stripping is achieved. The growth of Li dendrites and the decomposition of electrolyte are largely suppressed.

In this work, low-cost dual-salt LCEs composed of only 0.5 M Li salts (0.1 M LiDFP and 0.4 M LiBOB/LiFSI/LiTFSI) are proposed to develop LMBs with enhanced cycling stability. Reducing the content of Li salt definitely decreases the conductivity of the electrolyte. Considering the better wettability of LiFSI and LiTFSI toward PE separator, the conductivity decrement of the separator wetted by the electrolyte using these two salts is relatively mild. However, the conductivity of the

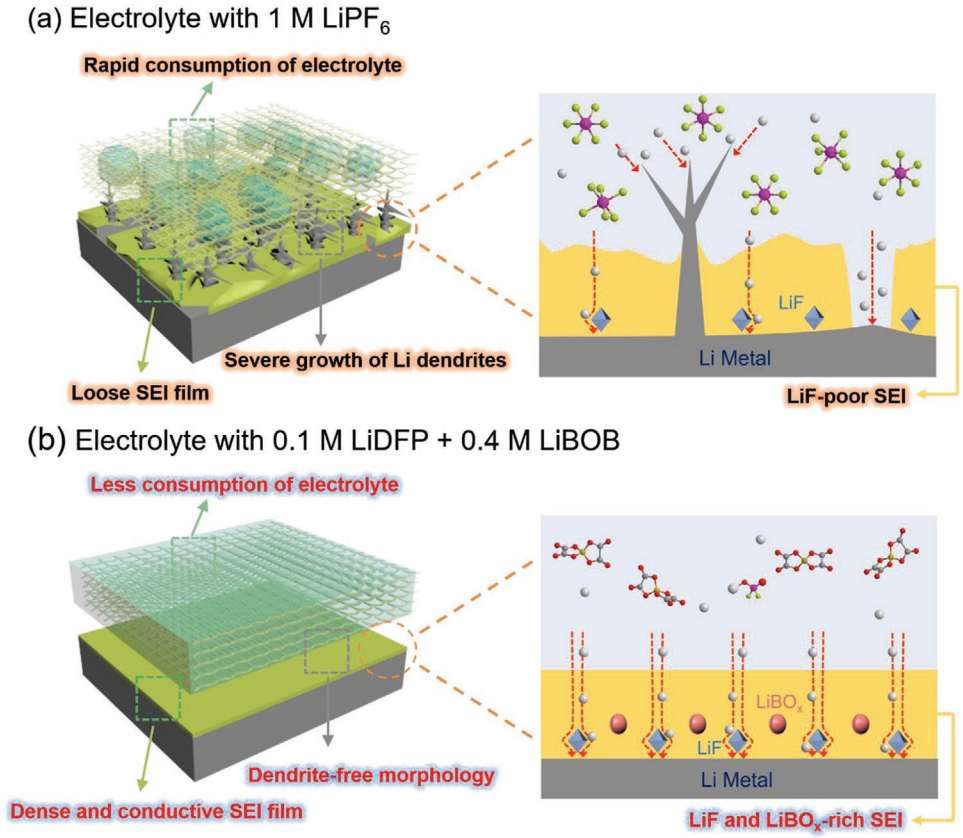

Figure 6. Schematic descriptions of Li plating progress in STD a) and b) D4B electrolytes.

wet separator in electrolyte using LiBOB is significantly lower than that of the conventional electrolyte. Frontier orbital energy calculations and XPS analyses indicate that LiDFP tends to be reduced to form an SEI film rich in LiF and phosphate compounds on the surface of Li metal. In addition, BOB^- also facilitates forming a flexible SEI film rich in Li_2BO_x. Growth of Li dendrites and parasitic reactions are effectively suppressed because of the high conductive and flexible SEI films. Significantly improved Li metal compatibility of the LCEs is verified from Li||Cu cells and Li||Li symmetric cells. The former showed that the accurate CE increased from 83.8% in STD electrolyte to over 93% in LCEs, and even reached 97.6% in D4B electrolyte, and the latter showed a stable cycling for more than 280 h. As a result, Li||LFP cells with moderate high cathode loading (2.0 mAh cm^{-2}) exhibit a capacity retention up to 95.4% after 300 cycles and the capacity even reaches 103.7 mAh g^{-1} at a current density of 16.0 mA cm^{-2} (8C rate) in D4B electrolyte. We believe our research provides new insights into developing new electrolytes with practical applicability toward LMBs.

Experimental Section

Theoretical Calculations: The HOMO and LUMO energies correlated with the oxidability and reducibility of molecules were calculated using Gaussian 09 package toward different anions and LiDFP. The density functional theory (DFT) of B3LYP and a basis set of 6-31G(d) was employed to optimize the geometry structure of molecules and a larger basis set of 6-311++G (d, p) was used to calculate the single point energy based on the polarizable continuum model (PCM).[34]

Electrodes and Electrolytes Preparation: $LiFePO_4$ (LFP) was supplied by Hefei Guoxuan High-Tech Power Energy Co., Ltd and Li metal (Φ 15.6 mm, 450 µm) was purchased from China Energy Lithium Co., Ltd. The solvents including EC and DMC were ordered from Shenzhen Capchem Technology Co., Ltd. The commercially available Li salts, including $LiPF_6$, LiDFP, LiBOB, LiFSI, and LiTFSI, were received from Guotai Super Power Co., Ltd.

The cathode was prepared by coating a slurry mixture of 84% LFP, 8% Super P conducting agent and 8% polyvinylidene fluoride (PVDF) binder in *N*-methyl-2-pyrrolidone on aluminum foil. After drying in vacuum at 80 °C for 12 h and pressed, the laminate was punched into disks with a diameter of 15.6 cm. The areal capacity of the cathode was 2.0 mAh cm^{-2}. Electrolytes were prepared by dissolving Li salts in EC/DMC (3:7 by weight ratio) in an argon-filled glove box (MBraun) with less than 0.1 ppm oxygen and moisture level. The amount of electrolyte added to each cell is 60 µL. The formula of the standard (STD) electrolyte and LCEs are as follows:

STD: 1 M $LiPF_6$ in EC/DMC (3:7, w/w)
D4B: 0.1 M LiDFP + 0.4 M LiBOB in EC/DMC (3:7, w/w)
D4F: 0.1 M LiDFP + 0.4 M LiFSI in EC/DMC (3:7, w/w)
D4T: 0.1 M LiDFP + 0.4 M LiTFSI in EC/DMC (3:7, w/w)

Physical and Electrochemical Measurements: Ionic conductivity of the electrolytes was directly measured on a DDS-307A conductivity meter (Leici, Shanghai) at different temperatures. The conductivity was fitted with VTF equation to obtain activation energy[31,35]

$$\sigma = \sigma_0 T^{-1/2} \exp\left[\frac{-E_0}{R(T-T_0)}\right] \quad (1)$$

where σ is the pre-exponential factor, E_a is the activation energy, T is the absolute temperature, and T_0 is the ideal glass transition temperature.

The Celgard 2730 polyethylene (PE) separator with a dimeter of 16 mm was used in this work. The electrolyte uptake and conductivity of the separator after immersed in the electrolyte for 2 h were calculated with following equations

$$\text{Electrolyte uptake} = \frac{(M - M_0)}{M_0} \times 100\% \quad (2)$$

$$\sigma_s = \frac{d}{A \times R_s} \quad (3)$$

$$\text{MacMullin number} = \frac{\sigma_e}{\sigma_s} \quad (4)$$

where M and M_0 are the weight of the separator with and without electrolyte, respectively, σ_s and σ_e represent the conductivity of the wet separator and electrolyte, respectively, d and A are corresponding to the thickness and contact area of the separator, and R_s is the impedance of the stainless steel (SS)|wet separator|SS symmetric cells, which can be obtained from the intercept of the Nyquist plot and x-axis.

The CR 2032 coin cells were used to evaluate the electrochemical performance of different electrolytes. All the cells were assembled and disassembled in the glove box and cycled on a LAND CT2100A test system in a constant temperature incubator. The accurate CE for different electrolyte was measured in Li||Cu cells according to the method 3 reported by Adams et al.[36] The cells were cycled at a constant current density of 0.4 mA cm^{-2}. First, the Cu substrate was pretreated with a single Li plating/stripping progress at a high capacity of 4 mAh cm^{-2} to form a stabilized surface passivation layer. Second, Li film of 4 mAh cm^{-2} was deposited on Cu foil served as Li reservoir. After that the cells were stripped and deposited for 10 cycles with an areal capacity of 0.8 mAh cm^{-2} (Q_C). Finally, the cells were charged to 1 V to strip all the deposited Li. The accurate CE was obtained with following equation

$$\text{CE} = \left(\frac{n \times Q_C + Q_S}{n \times Q_C + Q_T}\right) \times 100\% \quad (5)$$

where n is the cycle number, Q_S is the charge capacity of the final cycle, and Q_T is the capacity of the Li reservoir (4 mAh cm^{-2}).

The Li||LFP cells were cycled at 1C after two formation cycles at 0.1C between 2.5 and 3.8 V at room temperature (25 °C). Linear sweep voltammetry (LSV) was conducted using Pt as a working electrode and Li metal as both reference and counter electrodes at a scan rate of 0.5 mV s^{-2} on an CHI660e electrochemical workstation (Chenhua, Shanghai). AC impedance of Li||LFP cells was measured ranging from 0.01 Hz to 100 kHz at 5 mV amplitude. DC impedance (R_{DC}) was measured using a galvanostatic intermittent titration technique (GITT) on LAND CT200A test system.[37] In the DC impedance test, the current density was shifted from 1C to 0.5C. The cell was charged for 10 min and followed by a rest step for 40 minutes until the cell reached 3.8 V. The DC impedance was calculated with following equation

$$R_{DC} = \frac{\Delta U}{\Delta I} \quad (6)$$

where ΔU is the voltage difference before and after rest, and ΔI is the current density.

The transference number of Li^+ (t_+) was calculated according to the method proposed by Bruce and Bincent.[38] A small polarization overpotential (10 mV) was applied on Li||Li symmetric cells for 3600 s. The impedance before and after chronoamperometry test was also measured. The transference number was given by

$$t_+ = \frac{I_{SS}(\Delta V - I_0 R_0)}{I_0(\Delta V - I_{SS} R_{SS})} \quad (7)$$

where ΔV is the polarization overpotential (10 mV), I_0 and I_{SS} are the initial and steady-state current, R_0 and R_{SS} are the impedance before and after chronoamperometry test.

Material Characterizations: To explore the morphology of deposited Li, the Li||Li and Li||LFP cells were disassembled to retrieve the Li electrodes and the Cu foil with 1.5 mAh cm^{-2} Li film deposited on it was also retrieved from the Li||Cu cells. The Li and Li on Cu electrodes were rinsed with DMC for three times to remove the residual electrolyte. The surface and cross-section morphologies were examined using field-emission transmission electron microscope (FE-TEM, JEM-2100F). Ex situ XPS (America Thermo ESCALAB250) was conducted to reveal the chemical components of SEI layer.

Supporting Information

Supporting Information is available from the Wiley Online Library or from the author.

Acknowledgements

The authors appreciate the financial support of the National Key R&D Research Program of China (No. 2018YFB0905400), the National Science Foundation of China (Grant Nos. 51925207, 51872277, U1910210, 21676067, 51372060, and 21606065), Dalian National Laboratory For Clean Energy (DNL) Cooperation Fund, the CAS (DNL180310), and the Fundamental Research Funds for the Central Universities (JZ2017YYPY0253, WK2060140026, WK2060000009), (Natural Science Foundation of Anhui Province) Anhui Provincial Natural Science Foundation (1708085QE98), and the Opening Project of CAS Key Laboratory of Materials for Energy Conversion (KF2018003).

Conflict of Interest

The authors declare no conflict of interest.

Keywords

dual-salt, LiDFP, lithium-metal batteries, low concentration electrolytes, solid-electrolyte interphases

Received: April 27, 2020
Revised: June 4, 2020
Published online:

[1] D. Lin, Y. Liu, A. Pei, Y. Cui, *Nano Res.* **2017**, *10*, 4003.
[2] a) D. Lin, Y. Liu, Y. Cui, *Nat. Nanotechnol.* **2017**, *12*, 194; b) Y.-X. Yao, X.-Q. Zhang, B.-Q. Li, C. Yan, P.-Y. Chen, J.-Q. Huang, Q. Zhang, *InfoMat* **2020**, *2*, 379; c) B.-Q. Li, L. Kong, C.-X. Zhao, Q. Jin, X. Chen, H.-J. Peng, J.-L. Qin, J.-X. Chen, H. Yuan, Q. Zhang, J.-Q. Huang, *InfoMat* **2019**, *1*, 533.
[3] a) X.-Q. Zhang, X.-B. Cheng, X. Chen, C. Yan, Q. Zhang, *Adv. Funct. Mater.* **2017**, *27*, 1605989; b) Z. Peng, J. Song, L. Huai, H. Jia, B. Xiao, L. Zou, G. Zhu, A. Martinez, S. Roy, V. Murugesan, H. Lee, X. Ren, Q. Li, B. Liu, X. Li, D. Wang, W. Xu, J. G. Zhang, *Adv. Energy Mater.* **2019**, *9*, 1901764; c) F. Han, A. S. Westover, J. Yue, X. Fan, F. Wang, M. Chi, D. N. Leonard, N. J. Dudney, H. Wang, C. Wang, *Nat. Energy* **2019**, *4*, 187.
[4] a) Q. Zhou, S. Dong, Z. Lv, G. Xu, L. Huang, Q. Wang, Z. Cui, G. Cui, *Adv. Energy Mater.* **2020**, *10*, 1903441; b) S. Li, M. Jiang, Y. Xie, H. Xu, J. Jia, J. Li, *Adv. Mater.* **2018**, *30*, 1706375.

[5] a) S.-S. Chi, Y. Liu, W.-L. Song, L.-Z. Fan, Q. Zhang, *Adv. Funct. Mater.* **2017**, *27*, 1700348; b) T. Li, X.-Q. Zhang, P. Shi, Q. Zhang, *Joule* **2019**, *3*, 2647; c) Z. Hu, F. Xian, Z. Guo, C. Lu, X. Du, X. Cheng, S. Zhang, S. Dong, G. Cui, L. Chen, *Chem. Mater.* **2020**, *32*, 3405.

[6] a) D. Aurbach, A. Zaban, Y. Gofer, Y. E. Ely, I. Weissman, O. Chusid, O. Abramson, *J. Power Sources* **1995**, *54*, 76; b) J. Besenhard, M. Wagner, M. Winter, A. Jannakoudakis, P. Jannakoudakis, E. Theodoridou, *J. Power Sources* **1993**, *44*, 413; c) A. O. Bedenbaugh, J. H. Bedenbaugh, J. D. Adkins, W. Bergin, *J. Org. Chem.* **1970**, *35*, 543; d) H. Ota, Y. Sakata, Y. Otake, K. Shima, M. Ue, J.-i. Yamaki, *J. Electrochem. Soc.* **2004**, *151*, A1778; e) X. Ren, Y. Zhang, M. H. Engelhard, Q. Li, J.-G. Zhang, W. Xu, *ACS Energy Lett.* **2018**, *3*, 14.

[7] a) F. Ding, W. Xu, G. L. Graff, J. Zhang, M. L. Sushko, X. Chen, Y. Shao, M. H. Engelhard, Z. Nie, J. Xiao, X. Liu, P. V. Sushko, J. Liu, J.-G. Zhang, *J. Am. Chem. Soc.* **2013**, *135*, 4450; b) S.-J. Park, J.-Y. Hwang, Y.-K. Sun, *J. Mater. Chem. A* **2019**, *7*, 13441; c) S. Li, S. Fang, H. Dou, X. Zhang, *ACS Appl. Mater. Interfaces* **2019**, *11*, 20804; d) X. Shangguan, G. Xu, Z. Cui, Q. Wang, X. Du, K. Chen, S. Huang, G. Jia, F. Li, X. Wang, D. Lu, S. Dong, G. Cui, *Small* **2019**, *15*, 1970082; e) J. Dong, H. Dai, Q. Fan, C. Lai, S. Zhang, *Nano Energy* **2019**, *66*, 104128; f) G. Wan, F. Guo, H. Li, Y. Cao, X. Ai, J. Qian, Y. Li, H. Yang, *ACS Appl. Mater. Interfaces* **2018**, *10*, 593.

[8] a) P. Shi, H. Zheng, X. Liang, Y. Sun, S. Cheng, C. Chen, H. Xiang, *Chem. Commun.* **2018**, *54*, 4453; b) J. Yang, Z. Wang, Y. Shi, P. Sun, Y. Xu, *ACS Appl. Mater. Interfaces* **2020**, *12*, 7179; c) H. Jia, L. Zou, P. Gao, X. Cao, W. Zhao, Y. He, M. H. Engelhard, S. D. Burton, H. Wang, X. Ren, Q. Li, R. Yi, X. Zhang, C. Wang, Z. Xu, X. Li, J. G. Zhang, W. Xu, *Adv. Energy Mater.* **2019**, *9*, 1900784; d) J. Alvarado, M. A. Schroeder, M. Zhang, O. Borodin, E. Gobrogge, M. Olguin, M. S. Ding, M. Gobet, S. Greenbaum, Y. S. Meng, K. Xu, *Mater. Today* **2018**, *21*, 341.

[9] a) J. Wang, Y. Yamada, K. Sodeyama, C. H. Chiang, Y. Tateyama, A. Yamada, *Nat. Commun.* **2016**, *7*, 12032; b) J. Wang, Y. Yamada, K. Sodeyama, E. Watanabe, K. Takada, Y. Tateyama, A. Yamada, *Nat. Energy* **2018**, *3*, 22; c) L. Xiao, Z. Zeng, X. Liu, Y. Fang, X. Jiang, Y. Shao, L. Zhuang, X. Ai, H. Yang, Y. Cao, J. Liu, *ACS Energy Lett.* **2019**, *4*, 483; d) Z. Lin, Q. Xia, W. Wang, W. Li, S. Chou, *InfoMat* **2019**, *1*, 376.

[10] X. Ren, L. Zou, S. Jiao, D. Mei, M. H. Engelhard, Q. Li, H. Lee, C. Niu, B. D. Adams, C. Wang, J. Liu, J.-G. Zhang, W. Xu, *ACS Energy Lett.* **2019**, *4*, 896.

[11] S. Chen, J. Zheng, D. Mei, K. S. Han, M. H. Engelhard, W. Zhao, W. Xu, J. Liu, J.-G. Zhang, *Adv. Mater.* **2018**, *30*, 1706102.

[12] a) L. Yu, S. Chen, H. Lee, L. Zhang, M. H. Engelhard, Q. Li, S. Jiao, J. Liu, W. Xu, J.-G. Zhang, *ACS Energy Lett.* **2018**, *3*, 2059; b) X. Ren, L. Zou, X. Cao, M. H. Engelhard, W. Liu, S. D. Burton, H. Lee, C. Niu, B. E. Matthews, Z. Zhu, C. Wang, B. W. Arey, J. Xiao, J. Liu, J.-G. Zhang, W. Xu, *Joule* **2019**, *3*, 1662; c) N. Piao, X. Ji, H. Xu, X. Fan, L. Chen, S. Liu, M. N. Garaga, S. G. Greenbaum, L. Wang, C. Wang, X. He, *Adv. Energy Mater.* **2020**, *10*, 1903568; d) X. Ren, S. Chen, H. Lee, D. Mei, M. H. Engelhard, S. D. Burton, W. Zhao, J. Zheng, Q. Li, M. S. Ding, M. Schroeder, J. Alvarado, K. Xu, Y. S. Meng, J. Liu, J.-G. Zhang, W. Xu, *Chem* **2018**, *4*, 1877.

[13] J. Zheng, P. Yan, D. Mei, M. H. Engelhard, S. S. Cartmell, B. J. Polzin, C. Wang, J.-G. Zhang, W. Xu, *Adv. Energy Mater.* **2016**, *6*, 1502151.

[14] Y. Li, Y. Yang, Y. Lu, Q. Zhou, X. Qi, Q. Meng, X. Rong, L. Chen, Y.-S. Hu, *ACS Energy Lett.* **2020**, *5*, 1156.

[15] a) B. Ravikumar, M. Mynam, B. Rai, *J. Phys. Chem. C* **2018**, *122*, 8173; b) D. Rehnlund, C. Ihrfors, J. Maibach, L. Nyholm, *Mater. Today* **2018**, *21*, 1010.

[16] a) L. Qin, N. Xiao, J. Zheng, Y. Lei, D. Zhai, Y. Wu, *Adv. Energy Mater.* **2019**, *9*, 1902618; b) A. M. Colclasure, T. R. Tanim, A. N. Jansen, S. E. Trask, A. R. Dunlop, B. J. Polzin, I. Bloom, D. Robertson, L. Flores, M. Evans, E. J. Dufek, K. Smith, *Electrochim. Acta* **2020**, *337*, 135854.

[17] S. Jiao, X. Ren, R. Cao, M. H. Engelhard, Y. Liu, D. Hu, D. Mei, J. Zheng, W. Zhao, Q. Li, N. Liu, B. D. Adams, C. Ma, J. Liu, J.-G. Zhang, W. Xu, *Nat. Energy* **2018**, *3*, 739.

[18] H. Xiang, P. Shi, P. Bhattacharya, X. Chen, D. Mei, M. E. Bowden, J. Zheng, J.-G. Zhang, W. Xu, *J. Power Sources* **2016**, *318*, 170.

[19] J. Zheng, M. H. Engelhard, D. Mei, S. Jiao, B. J. Polzin, J.-G. Zhang, W. Xu, *Nat. Energy* **2017**, *2*, 17012.

[20] a) C. Wang, L. Yu, W. Fan, J. Liu, L. Ouyang, L. Yang, M. Zhu, *ACS Appl. Energy Mater.* **2018**, *1*, 2647; b) K.-E. Kim, J. Y. Jang, I. Park, M.-H. Woo, M.-H. Jeong, W. C. Shin, M. Ue, N.-S. Choi, *Electrochem. Commun.* **2015**, *61*, 121.

[21] P. Shi, L. Zhang, H. Xiang, X. Liang, Y. Sun, W. Xu, *ACS Appl. Mater. Interfaces* **2018**, *10*, 22201.

[22] a) Y. Xie, H. Zou, H. Xiang, R. Xia, D. Liang, P. Shi, S. Dai, H. Wang, *J. Membr. Sci.* **2016**, *503*, 25; b) P. Arora, Z. Zhang, *Chem. Rev.* **2004**, *104*, 4419.

[23] H. Zheng, X. Zhou, S. Cheng, R. Xia, S. P. Nie, X. Liang, Y. Sun, H. F. Xiang, *J. Electrochem. Soc.* **2019**, *166*, A1456.

[24] A. Terella, F. De Giorgio, M. Rahmanipour, L. Malavolta, E. Paolasini, D. Fabiani, M. L. Focarete, C. Arbizzani, *J. Power Sources* **2020**, *449*, 227556.

[25] Y. Xie, H. Xiang, P. Shi, J. Guo, H. Wang, *J. Membr. Sci.* **2017**, *524*, 315.

[26] Q. Wang, Z. Cui, Q. Zhou, X. Shangguan, X. Du, S. Dong, L. Qiao, S. Huang, X. Liu, K. Tang, X. Zhou, G. Cui, *Energy Storage Mater.* **2020**, *25*, 756.

[27] a) H. Fujimoto, S. Satoh, *J. Phys. Chem.* **1994**, *98*, 1436; b) C. G. Zhan, J. A. Nichols, D. A. Dixon, *J. Phys. Chem. A* **2003**, *107*, 4184.

[28] a) G. G. Eshetu, G. A. Elia, M. Armand, M. Forsyth, S. Komaba, T. Rojo, S. Passerini, *Adv. Energy Mater.* **2020**, *10*, 2000093; b) M. D. Halls, K. Tasaki, *J. Power Sources* **2010**, *195*, 1472.

[29] X. Shen, R. Zhang, X. Chen, X. B. Cheng, X. Li, Q. Zhang, *Adv. Energy Mater.* **2020**, *10*, 1903645.

[30] X.-Q. Zhang, T. Li, B.-Q. Li, R. Zhang, P. Shi, C. Yan, J.-Q. Huang, Q. Zhang, *Angew. Chem.* **2020**, *132*, 3278; XXXX, *Angew. Chem., Int. Ed.* **2020**, *59*, 3252.

[31] K. Xu, *Chem. Rev.* **2004**, *104*, 4303.

[32] Q. Zhang, K. Wang, X. Wang, Y. Zhong, M. Liu, X. Liu, K. Xu, W. Fan, L. Yu, W. Li, *ACS Appl. Mater. Interfaces* **2019**, *11*, 20854.

[33] a) T. Jaumann, J. Balach, M. Klose, S. Oswald, J. Eckert, L. Giebeler, *J. Electrochem. Soc.* **2016**, *163*, A557; b) Z. Hu, S. Zhang, S. Dong, Q. Li, G. Cui, L. Chen, *Chem. Mater.* **2018**, *30*, 4039.

[34] a) X. Cao, X. Ren, L. Zou, M. H. Engelhard, W. Huang, H. Wang, B. E. Matthews, H. Lee, C. Niu, B. W. Arey, Y. Cui, C. Wang, J. Xiao, J. Liu, W. Xu, J.-G. Zhang, *Nat. Energy* **2019**, *4*, 796; b) B. Liu, Q. Li, M. H. Engelhard, Y. He, X. Zhang, D. Mei, C. Wang, J.-G. Zhang, W. Xu, *ACS Appl. Mater. Interfaces* **2019**, *11*, 21496.

[35] S.-H. Wang, Y.-Y. Lin, C.-Y. Teng, Y.-M. Chen, P.-L. Kuo, Y.-L. Lee, C.-T. Hsieh, H. Teng, *ACS Appl. Mater. Interfaces* **2016**, *8*, 14776.

[36] B. D. Adams, J. Zheng, X. Ren, W. Xu, J.-G. Zhang, *Adv. Energy Mater.* **2018**, *8*, 1702097.

[37] M. Wang, X. Feng, H. Xiang, Y. Feng, C. Qin, P. Yan, Y. Yu, *Small Methods* **2019**, *3*, 1900355.

[38] J. Evans, C. A. Vincent, P. G. Bruce, *Polym. Plast. Technol. Eng.* **1987**, *28*, 2324.